Penetration Loss Analysis for mmWave MIMO Communication in Indoor Environments

Hyunsoo Lee, Hanvit Kim, Hyeonjin Chung, Keonho Cha, and Sunwoo Kim
Department of Eletronic Engineering, Hanyang University, Seoul, South Korea
{geniusoo, dante0813, hyeonjingo, crjsgh, remero}@hanyang.ac.kr

***Abstract*—This paper presents the penetration loss of different materials for indoor millimeter-wave (mmWave) communication. The measurements of penetration loss were conducted in indoor environments via the mmWave multiple-input multiple-output (MIMO) testbed. The mmWave MIMO testbed consists of the NI PXI platforms, the TMYTEK mixer, and the TMYTEK uniform planar array antenna. The experiment was conducted with several materials, such as tinted glass and plywood-based partitions, that could be commonly found in indoor environments. The results show that the tinted glass has higher penetration loss than plywood-based partitions due to the density and surface of the material.**

***Keywords*—Penetration loss, mmWave testbed, MIMO, channel sounding, indoor**

I. Introduction

The millimeter-wave (mmWave) and terahertz (THz) bands in indoor environments suffer from relatively severe propagation and penetration losses that impair communication performance. Predicting the penetration loss is one of the challenges in indoor mmWave communications. To achieve stable communication performance in indoor environments, measuring the penetration loss of several materials and the analysis is essential. However, the implementation of a real time mmWave testbed system for measuring penetration loss significantly suffer due to several problems such as expenses, hardware imperfections, complicated control, and many radio frequency (RF) analog components.

Even with those problems, there are several studies for measuring penetration loss in indoor environments. Authors in [1] defined the mathematical model of 5G/6G mmWave and THz cellular systems, and they also suggested propagation models such as ray-tracing and the measurement data-based model. In [2], they presented propagation measurement results and the penetration loss measurements of the mmWave (28 and 73 GHz) and sub-THz (140 GHz). In [3], the penetration loss and attenuation measurements for different materials of mmWave and sub-THz band in the line-of-sight (LOS) and non-line-of-sight (NLOS) scenarios were conducted at the North Carolina State University, Raleigh, NC. And, the study for measuring the penetration loss and reflection coefficient in common building materials of 28 GHz was performed in the New York urban environment [4]. Furthermore, in [5], the authors measured the wideband penetration loss of 73 GHz at New York University, which can be considered a typical office environment.

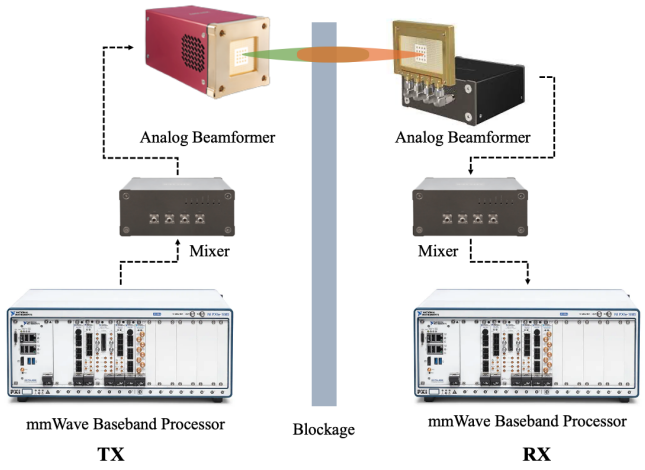

Figure 1. mmWave MIMO testbed setup for measuring penetration loss.

As the previous studies suggest, measuring the penetration loss is important for mmWave communications. The penetration loss is affected by many complex factors, such as measurement setup, the distance between the transmitter (TX) and receiver (RX), the experiment environment, and types of blockage materials. Further results for measuring the penetration loss in indoor environments are needed to design the channel model of mmWave and THz band. Thus, we present the 28 GHz mmWave multiple-input multiple-output (MIMO) testbed and measure the penetration loss of different materials that can be found in general indoor environments.

II. Experimental Setup

In this section, we suggest the MIMO channel sounder configuration and experimental environments. The architecture of the MIMO penetration loss measurement is described in Figure 1. The existing works for measuring the penetration was conducted via horn antenna [2]–[5]. A horn antenna is significantly used for radar systems by concentrating the radio waves, and it can reduce multipath interference and accommodate the wide bandwidth through polarization techniques [6]. The mmWave systems require an antenna that is capable of processing signals in various directions to overcome multipath fading, shadow effects, and interference polarization [2], [6], [7].

TABLE I. Specifications of the MIMO channel sounder

Parameters	Value
Radio frequency	28 GHz
Bandwidth	800 MHz
Sampling frequency	3.072 GS/s
Waveform	CP-OFDM
FFT size(/bin spacing)	2048 (@ 75 kHz subcarrier spacing)
Antenna size	TX: 4×4; RX: 1×4
MIMO Scheme	Analog beamforming
Modulation	64-QAM
Coding	Turbo
Throughput	3 Gbps (Maximum)

A. MIMO Channel Sounder Configuration

The channel sounder consists of the National Instruments (NI) PCI extensions for Instrumentation (PXI) platforms [8], the TMYTEK RF converter [9], and the TMYTEK uniform planar array (UPA) antennas [10], [11].

The NI PXI platform of the TX side includes PXIe-7902 FPGA processors, a PXIe-3610 processor, a PXIe-3620 processor, a PXIe-1085 chassis, and a PXIe-8880 embedded controller. The PXIe-7902 performs digital signal processing as below digital modulation and channel coding required for wireless communication and sends the digital data to the PXIe-3610. The PXIe-3610 is a digital-to-analog converter processor, which generates the baseband signal according to the digital data from PXIe-7902, and sends the baseband signal to the PXIe-3620. The PXIe-3620 is a local oscillator processor, which up-converts the baseband signal to 10.56 GHz intermediate frequency (IF), and sends the IF signals to the RF converter. All of the processors are commonly connected with PXIe-8880 and PXIe-1085 and controlled via LabVIEW. The LabVIEW software is a graphical programming environment used to develop automated research, validation, and production test system. The NI PXI platform on the RX side is configured with the same specifications as the TX side, and the difference is an analog-to-digital converter PXIe-3630 processor substitute for the PXIe-3610. The RF converter up-converts the IF signals to 28 GHz mmWave, and the UPA antenna radiates the 28 GHz mmWave signal to the desired direction. The UPA antenna has robustness to multipath fading, shadow effects, and interference polarization. The system specifications of the MIMO channel sounder are summarized in Table I, and the detailed configurations are given in Figure 2.

B. Measurement Environments

Measurements for the penetration loss were conducted in the 5G Unmanned Vehicle Research Center, located on the 5$^{\text{th}}$ floor of the Fusion Technology Center, Hanyang University, Seoul, South Korea. The measurement location is similar to a prevalent indoor office environment that includes common interior materials such as glass, wooden desks, partitions, and drywalls. We configured the measurement environments as the LOS and NLOS scenario by changing the distance between the TX and RX. Distances of each scenario were initially set to 60 cm, progress last to 140 cm, and the resolution of the distance was 10 cm. In the LOS scenario, we configured the environment without a blockage. In the NLOS scenario, we conducted environments with different blockages, such as the tinted glass and plywood-based partitions, respectively. The tinted glass is coated on one side, and the plywood-based partitions are covered by fabrics and plastic frames. The dimension and thickness of each blockage are described in Table II.

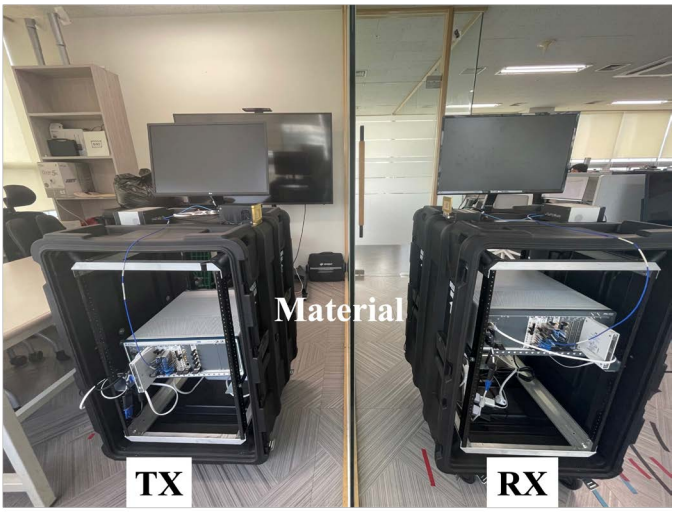

Figure 2. Experimental setup and environments.

III. Penetration Loss Results and Analysis

In this section, we introduce the procedure of the penetration loss measurement, the results, and the analysis. The measurement procedure consists of several steps in the LOS and NLOS scenario.

A. Measurement Procedure

The procedure for measuring penetration loss is presented as follows: we aligned the TX and RX with a straight line without any blockage and measured the average received power in the LOS scenario. Then, we measured the average received power after assigning a blockage between the TX and RX and the same alignment in the NLOS scenario. The average received power in the LOS scenario $P_{r,\text{LOS}}$, in the NLOS scenario $P_{r,\text{NLOS}}$, and the free space penetration loss (FSPL), can be calculated as [12], [13]:

$$P_{r,\text{LOS}}\ (\text{dB}) = P_t + G_t + G_r - \text{FSPL}\ , \tag{1}$$

$$P_{r,\text{NLOS}}\ (\text{dB}) = P_t + G_t + G_r - \text{FSPL} - \text{PL}_{\text{material}}\ , \tag{2}$$

$$\text{FSPL} = 20\log_{10}\left(\frac{4\pi df}{c}\right) - G_t - G_r\ , \tag{3}$$

where, P_t is the TX transmit power in dBm, G_t is the TX antenna gain in dBi, G_r is the RX antenna gain in dBi,

TABLE II. Dimension and thickness of blockages.

Material	Width (cm)	Height (cm)	Thickness (cm)
Tinted glass	373.21	272.74	0.12
Plywood-based partition	77.57	112.91	3.36

TABLE III. Results of average received power and penetration loss for tinted glass and plywood-based partitions.

Distance (cm)	**60**	**70**	**80**	**90**	**100**	**110**	**120**	**130**	**140**
$P_{r,\,\mathrm{LOS}}$ (dBm)	-44.556	-45.952	-47.127	-49.511	-50.553	-51.368	-52.871	-53.642	-54.785
$P_{r,\,\mathrm{glass}}$ (dBm)	-50.741	-51.708	-52.674	-53.996	-54.981	-55.813	-56.819	-58.223	-60.456
$P_{r,\,\mathrm{partition}}$ (dBm)	-49.712	-50.147	-51.433	-51.962	-52.657	-52.959	-53.637	-54.812	-56.337
$\mathrm{PL}_{\mathrm{glass}}$(dB)	6.185	5.756	5.547	4.485	4.448	4.445	4.002	4.581	5.671
$\mathrm{PL}_{\mathrm{partition}}$(dB)	5.156	4.195	4.306	2.451	2.104	1.591	0.766	1.170	1.552

$\mathrm{PL}_{\mathrm{material}}$ is the penetration loss of a material, d is the distance between TX and RX, f is the radio frequency, c is the speed of light in free space.

The penetration loss is defined by the received power of the LOS scenario and NLOS scenario at the same distance for each material. The penetration loss of a material, $\mathrm{PL}_{\mathrm{material}}$, can be calculated by:

$$\mathrm{PL}_{\mathrm{material}}(\mathrm{dB}) = P_{r,\mathrm{LOS}} - P_{r,\mathrm{NLOS}} \ . \tag{4}$$

B. Results and Analysis

Table III provides the results of the average received power and penetration loss of all materials for every distance, respectively. The measurement results of the average received power of tinted glass and plywood-based partitions are denoted by $P_{r,\mathrm{glass}}$ and $P_{r,\mathrm{partition}}$. The penetration loss of tinted glass and plywood-based partitions are denoted by $\mathrm{PL}_{\mathrm{glass}}$ and $\mathrm{PL}_{\mathrm{partition}}$, respectively. For the tinted glass, the results of penetration loss are higher than the plywood-based partitions scenario, at all distances. The maximum penetration loss of tinted glass was at 6.185 dB in the 60 cm. In the 120 cm distance, the penetration loss was the lowest at 4.002 dB in the results of tinted glass. The maximum and lowest penetration loss of plywood-based partitions were at 5.516 dB and 0.766 dB in the 60 cm and 120 cm, respectively, same as the distance of the tinted glass. The average penetration loss of tinted glass is 5.005 dB, and the average penetration loss of plywood-based partitions is 2.587 dB.

The results of average received power results for all materials steadily decreased when the separation distances increased. The penetration loss results of tinted glass for all distances are higher than the plywood-based partitions, even though tinted glass is more thin. Also, the average penetration loss of tinted glass is higher than plywood-based partitions. The similar results of the penetration loss of tinted glass in the distance 90 cm to 110 cm could be explained by the uneven surface, coated on one side, causing the diffuse reflection and the high diffraction loss of the incident ray of RX. The high penetration loss of tinted glass is due to the characteristics of the material, such as the high density, rough surface, and constituent matter.

IV. Conclusion

This paper presents the measurements of penetration loss of common indoor materials using 28 GHz mmWave MIMO. The penetration loss was measured by subtracting the average received power in NLOS conditions from LOS conditions. We employed tinted glass and plywood-based partitions for the experimental materials. Penetration loss results of all materials showed a tendency to gradually decrease up to 120 cm. The experiment results show that the high penetration loss of tinted glass was verified in indoor environments throughout the work. These results will be applied to the mmWave and THz research, such as integrated sensing and communications demonstration for indoor and blockage environments.

Acknowledgment

This work was supported by the National Research Foundation of Korea (NRF) grant funded by the Korea government (MSIT) (No. NRF-2023R1A2C3002890).

References

[1] D. Moltchanov *et al.*, "A tutorial on mathematical modeling of 5G/6G millimeter wave and terahertz cellular systems," *IEEE Commun. Surv. Tut.*, vol. 24, no. 2, pp. 1072–1116, Mar. 2022.

[2] T. S. Rappaport *et al.*, "Wireless communications and applications above 100 GHz: Opportunities and challenges for 6G and beyond," *IEEE Access*, vol. 7, pp. 78 729–78 757, Jun. 2019.

[3] K. Du, O. Ozdemir, F. Erden, and I. Guvenc, "Sub-terahertz and mmWave penetration loss measurements for indoor environments," in *Proc. 2021 IEEE Int. Conf. Commun. Workshops (ICC Workshops). IEEE*, Jun. 2021, pp. 1–6.

[4] H. Zhao *et al.*, "28 GHz millimeter wave cellular communication measurements for reflection and penetration loss in and around buildings in New York city," in *Proc. 2013 IEEE Int. Conf. Commun. (ICC). IEEE*, Jun. 2013, pp. 5163–5167.

[5] J. Ryan, G. R. MacCartney, and T. S. Rappaport, "Indoor office wideband penetration loss measurements at 73 GHz," in *Proc. 2017 IEEE Int. Conf. Commun. Workshops (ICC workshops). IEEE*, May 2017, pp. 228–233.

[6] W. L. Stutzman and G. A. Thiele, *Antenna theory and design*. John Wiley & Sons, 2012.

[7] Y. Niu, Y. Li, D. Jin, L. Su, and A. V. Vasilakos, "A survey of millimeter wave communications mmWave for 5G: opportunities and challenges," *Wirel. Net.*, vol. 21, pp. 2657–2676, Apr. 2015.

[8] NI, "mmWave Transceiver System," National Instruments, Tech. Rep., Jul. 2018. [Online]. Available: https://www.ni.com/en-us/shop/wireless-design-test/what-is-mmwave-transceiver-system.html

[9] TMYTEK, "UDBox 5G," TMYTEK, Tech. Rep., Nov. 2022, verison 1.0.8. [Online]. Available: https://www.tmytek.com/products/frequency-converters/udbox5g

[10] TMYTEK, "BBox 5G One," TMYTEK, Tech. Rep., Oct. 2022, version 1.0.8. [Online]. Available: https://www.tmytek.com/products/beamformers/bbox

[11] TMYTEK, "BBox 5G Lite," TMYTEK, Tech. Rep., Oct. 2022, version 1.4.7. [Online]. Available: https://www.tmytek.com/products/beamformers/bbox

[12] J. D. Parsons and P. J. D. Parsons, *The mobile radio propagation channel*. Wiley New York, 2000, vol. 2.

[13] H. Hashemi, "The indoor radio propagation channel," *Proc. IEEE*, vol. 81, no. 7, pp. 943–968, Jul. 1993.